OPEN ACCESS

UNIVERSITY OF DUNDEE

University of Dundee

A new model for root growth in soil with macropores

Landl, Magdalena; Huber, Katrin; Schnepf, Andrea ; Vanderborght, Jan; Javaux, Mathieu; Bengough, A. Glyn; Vereecken, Harry

Link to publication in Discovery Research Portal

A new model for root growth in soil with macropores

2 Magdalena Landl (1)*, Katrin Huber (1), Andrea Schnepf (1), Jan Vanderborght (1), Mathieu Javaux (1, 2), A. Glyn

3 Bengough (3, 4) and Harry Vereecken (1)

4

5 **Affiliations**

6 (1) Forschungszentrum Juelich GmbH, Agrosphere (IBG-3), D- 52428 Juelich, Germany

7 (2) Earth and Life Institute/ Environmental Sciences, Université catholique de Louvain, B-1348 Louvain-la-Neuve,

8 Belgium

9 (3) The James Hutton Institute, Invergowrie, Dundee, DD2 5DA, UK

10 (4) School of Science and Engineering, University of Dundee, Dundee DD1 4HN, UK.

11

12 *Corresponding author:

13 Magdalena Landl

14 Forschungszentrum Juelich GmbH, Agrosphere (IBG-3)

15 D- 52428 Juelich, Germany

16 Tel.: +49 2461 61 8835

17 Fax: +49 2461/61 2518

18   m.landl@fz-juelich.de

19

20 Number of text pages: 24

21 Number of tables: 3

22 Number of figures: 15

25

26   **Abstract**

27   *Background and Aims* The use of standard dynamic root architecture models to simulate root growth in soil

28   containing macropores failed to reproduce experimentally observed root growth patterns. We thus developed a new,

29   more mechanistic model approach for the simulation of root growth in structured soil.

30   *Methods* In our alternative modelling approach, we distinguish between, firstly, the driving force for root growth,

31   which is determined by the orientation of the previous root segment and the influence of gravitropism and, secondly,

32   soil mechanical resistance to root growth. The latter is expressed by its inverse, soil mechanical conductance, and

33   treated similarly to hydraulic conductivity in Darcy's law. At the presence of macropores, soil mechanical

34   conductance is anisotropic, which leads to a difference between the direction of the driving force and the direction of

35   the root tip movement.

36   *Results* The model was tested using data from the literature, at pot scale, at macropore scale, and in a series of

37   simulations where sensitivity to gravity and macropore orientation was evaluated.

38   *Conclusions* Qualitative and quantitative comparisons between simulated and experimentally observed root systems

39   showed good agreement, suggesting that the drawn analogy between soil water flow and root growth is a useful one.

40

2

Introduction

42 Due to high bulk densities in the subsoil, roots preferentially grow in the topsoil layer, where soil penetration

43 resistance is low (Ehlers et al. 1983b; Gregory 2008). There is, however, evidence that a significant amount of plant

44 available nutrients as well as water supplies are stored in the subsoil. Especially during drought periods or when the

45 top soil layer is nutrient depleted these subsoil resources play an important role in plant nutrition and can help to

46 reduce the amount of irrigation water and fertilizer needed (Gaiser et al. 2013; Kautz et al. 2013a; Kirkegaard et al.

47 2007).

48 The extent to which plants take up nutrients and water from the subsoil essentially depends on the fraction of roots

49 that are able to penetrate this hard soil layer (Kuhlmann and Baumgärtel 1991). A possibility for roots to gain access

50 to deeper, highly dense soil horizons is to use large sized macropores (diameters > 2 mm) as preferential pathways

51 (Ehlers et al. 1983a; Kautz et al. 2013b; McKenzie et al. 2009; Stewart et al. 1999; Stirzaker et al. 1996). The

52 probability of roots to grow in macropores depends on the abundance of pores in the soil (Hatano et al. 1988) and on

53 the penetration resistance of the bulk soil (Hirth et al. 2005). While some studies (Stewart et al. 1999; Stirzaker et al.

54 1996) observed that significantly more roots encountered macropores than what would be expected if root growth

55 was purely random, others (Dexter 1986; McKenzie et al. 2009) assume that roots locate macropores only by chance.

56 Kautz et al. (2013b) observed that roots use macropores to overcome hard soil layers, but then again re-enter the bulk

57 soil. This is in line with the results by Hirth et al. (2005) who found roots to grow more frequently in macropores

58 when the bulk density is higher. Dexter and Hewitt (1978), Stirzaker et al. (1996) and Hirth et al. (2005) observed

59 that roots tend to grow over a longer distance in macropores that are aligned more vertically. Hatano et al. (1988),

60 Stirzaker et al. (1996) and Valentine et al. (2012) have shown that root elongation in macropores is higher than in the

61 surrounding bulk soil.

62 Roots do not only use macropores as preferential pathways, but also take up nutrients from the pore walls, which

63 were observed to be rich in nutrients (Athmann et al. 2014). Due to the generally low water content inside

64 macropores when soil is dry (Laloy et al. 2010), root water uptake from the pore walls is vital (White and Kirkegaard

65 2010). Knowledge about the root – macropore – soil contact is thus essential. Athmann et al. (2013) have shown that

66 the way roots connect to the pore wall depends on the plant genotype. White and Kirkegaard (2010) and Kautz and

67 Köpke (2009) found most roots to grow straight through the pore and connect to the pore wall by the help of root

3

68 hairs respectively lateral branches if they do not have direct contact. Athmann et al. (2013) observed that barley roots

69 spiral down in large coils inside the pore wall. Field studies have shown that 85 % of the roots of a barley and oilseed

70 rape crop, which were found in macropores established contact to the pore wall (Athmann et al. 2013).

71 These plant scale observations converge with our current understanding how environmental stimuli influence root

72 growth. Toyota and Gilroy (2013) physiologically analyzed the mechanisms of gravitropic and mechanical signaling

73 in roots. Shkolnik et al. (2016) state the importance of hydrosensing, where roots grow away from low water

74 potential towards higher water potential. Bao et al. (2014) observed that the formation of lateral roots depends on the

75 availability of water in the vicinity of the root.

76 The influence of macropores on root growth as well as on root water and nutrient uptake from the subsoil is hard to

77 measure directly. Simulation models that describe root development in structured soils and water and nutrient fluxes

78 in the root zone are therefore useful tools to interpret measurements that provide indirect information about uptake

79 processes, e.g. soil water contents, plant nutrient contents and water and nutrient isotopic profiles in the soil and in

80 the plant. Until now, only few models exist, which include the responses of roots to macropores (Vereecken et al.

81 2016). Gaiser et al. (2013) modeled the effect of macropores on root development at the plot scale and Jakobsen and

82 Dexter (1988) investigated the influence of macropores on root growth and water uptake in a water balance model. In

83 these model simulations, the amount of roots that grow into macropores was prescribed or parameterized. But how

84 this parameterization changes with changing soil properties (e.g. matric bulk density, amount and orientation of

85 macropores) and root growth parameters (e.g. root growth responses to soil penetration resistance, gravity) cannot be

86 predicted by these models but is required model input. Such predictions require explicit simulation of root growth

87 and development at both the single root and the root system scale.

88 In recent years, several different simulation models for the description of growing root systems have been developed.

89 While the early models merely focused on the representation of the root system architecture, the later models are

90 more complex and also include the influence of the surrounding soil. Most of these later models (Clausnitzer and

91 Hopmans 1994; Pagès et al. 2004) calculate the rate and direction of root growth as the vector sum of various root

92 segment length and direction-affecting components. Root growth models frequently use the concept of tropisms to

93 represent the influence of plant physiological properties on the direction of root growth. The gradient of the

94 environmental stimulus that triggers a certain tropism defines the direction in which the root tip will grow. Most root

4

95   growth models include the influence of gravitropism (Clausnitzer and Hopmans 1994; Leitner et al. 2010; Pagès et

96   al. 2004) and some also take into account chemotropism and hydrotropism (Leitner et al. 2010; Tsutsumi et al.

97   2003). The effect of soil heterogeneities on the direction of root growth is typically implemented similarly to the

98   concept of tropisms: The gradient of soil mechanical resistance defines the direction of root growth, i.e. roots grow in

99   the direction in which the soil resistance decreases most rapidly (Clausnitzer and Hopmans 1994; Pagès et al. 2004).

100 The influence of soil mechanical resistance on the root growth direction is controlled by a sensitivity factor.

101 However, using this 'tropism approach', we were not able to simulate root growth along the macropore wall or to

102 simulate the way that roots appear to 'find' macropores in deeper soil layers and grow into them. Whilst the

103 approach is logical and attractive in simulating root growth in bulk soil, it needs to be modified to enable the

104 simulation of root growth in, along, and out of macropores. This is primarily due to large gradients in strength,

105 geometry, and matric potential that change rapidly adjacent to macropore walls. Therefore, a more mechanistic

106 description of root growth to determine the root growth direction seems necessary.

107 This study presents a new method for computing root growth in soils with macropores. It distinguishes between the

108 driving forces for root growth and anisotropy of soil strength, which is similar to the description of water flow in a

109 soil with anisotropic hydraulic conductivity. The new 'anisotropy approach' is illustrated by the simulation of an

110 experimental study by Stirzaker et al. (1996) on root growth in artificial macropores. Experimental and simulation

111 results using both the tropism and anisotropy approach to model changes in root growth direction are compared

112 visually and quantitatively. The potential of the anisotropy approach to simulate the effects of different macropore

113 inclination angles, bulk soil penetration resistances, and gravitropism on root growth in structured soil are

114 demonstrated by comparing simulation results with experimental data from Hirth et al. (2005). To evaluate its

115 performance on root growth in a multi – layered soil domain containing macropores, we carried out a simulation

116 study that was inspired by an experimental study by Dexter (1986).

117 **Material and Methods**

118 Model description

119 In our new approach, we draw an analogy between the movement of a root tip and water flow in porous media (Bear

120 2013). The root tip is pushed by a root inherent driving force into the soil. The direction of this driving force depends

121 on the direction of the previous root segment and on a gravitational component that is directed downwards. This

5

122 driving force is counteracted by soil mechanical forces and friction. If the friction force depends on the direction of

123 the movement, i.e. when the friction or soil resistance is anisotropic, the movement of the root tip will deviate from

124 the direction of the driving force.

125 In analogy with soil water flow, the direction of the root tip movement corresponds to the water flux vector, while

126 the driving force represents the gradient of the water potential. Soil mechanical forces can be seen as the viscous

127 friction forces that counteract water flow and thus the driving force. In the Darcy equation, the effect of these viscous

128 forces on energy dissipation is represented by the hydraulic conductance tensor, which may show anisotropy.

129 Analogous to the Darcy flow equation, we express the movement of the root tip by the following equation:

$$\mathbf{d} = \mathbf{k} \cdot \mathbf{F}, \tag{1}$$

130

131 where $\mathbf{d}$ is root tip movement vector, $\mathbf{k}$ is the soil mechanical conductance tensor that represents the ease with which

132 the root can penetrate the soil and $\mathbf{F}$ is the driving force that influences the root growth direction.

133 The soil mechanical conductance tensor $\mathbf{k}$ is a symmetric, second rank tensor with nine entry values defining

134 conductances in the three principal directions:

$$\mathbf{k} = \begin{pmatrix} k_{xx} & k_{xy} & k_{xz} \\ k_{yx} & k_{yy} & k_{yz} \\ k_{zx} & k_{zy} & k_{zz} \end{pmatrix}. \tag{2}$$

135

136 For an isotropic soil domain, where soil penetration resistance, or conductance as its inverse, is uniform in each

137 direction, the conductance tensor $\mathbf{k}$ can be reduced to a diagonal matrix in which all diagonal entry values are

138 identical. The direction of movement of the root tip then merely depends on the driving force. The simplest example

139 of soil heterogeneity is a stratified soil domain where each layer has a different conductance. In accordance with soil

140 hydraulic conductivity, the soil mechanical conductance in direction of the soil layering equals the arithmetic mean

141 whereas the conductance perpendicular to the soil layering is equal to the harmonic mean of the individual soil layer

142 conductances. If the direction of the soil layers, i.e. the axis of anisotropy, coincides with one of the axes of the

143 Cartesian coordinate system, the conductance tensor is a diagonal matrix with three different entry values. If the

144 layering or the axes of anisotropy are not aligned with the Cartesian coordinate system, the conductance tensor $\mathbf{k}$ is

145 fully occupied with nine entry values. In an anisotropic medium, the root tip movement deviates from the direction

146 of the driving force and is oriented towards the axis of anisotropy in which the conductance is largest and resistance

6

147   is smallest. Anisotropy in the soil domain can be caused by macropores, soil aggregation or differently compacted

148   soil layers. Furthermore, local differences in soil water content e.g. due to root water uptake, also lead to anisotropy

149   and affect the direction of root growth. Unlike the approaches by Clausnitzer and Hopmans (1994) and Pagès et al.

150   (2004), no sensitivity factor is needed to weigh the influence of penetration resistance on the root growth direction.

151   The driving force **F** could comprise several factors. We chose here the direction vector of the previous root segment

152   and gravitropism. The direction of the previous root segment is expressed by the azimuth angle α and the polar angle

153   β. To account for small scale variations in the soil matrix and to represent a random behavior of the root tip, random

154   deflection angles γ and δ are added to α and β (Fig. 1).

155
$$F = \begin{pmatrix} dx_{(\alpha,\beta,\gamma,\delta)} \\ dy_{(\alpha,\beta\gamma,\delta)} \\ dz_{(\alpha,\beta\gamma,\delta)} \end{pmatrix} + sg \begin{pmatrix} 0 \\ 0 \\ -1 \end{pmatrix}; \tag{3}$$

156   While the first term on the right hand side of equation (3) represents the previous growth direction vector of F, the

157   second term expresses the gravitropism component with sg as gravitropism sensitivity factor.

158   While the deflection of the azimuth angle γ is a uniformly distributed random angle between [0 2π], the deflection of

159   the polar δ is a normally distributed random angle with mean zero and standard deviation σ_{dl}, which is calculated

160   following the approach by Leitner et al. (2010). The standard deviation σ_{dl} is derived from the user defined unit

161   standard deviation σ of a root segment of 1 cm length and the maximum root segment length dl, which is reached

162   when soil penetration resistance equals zero. In probability theory, standard deviation decreases by the square root of

163   the number of trials. If 1/dl (segments per cm) is regarded as the number of trials, the standard deviation σ_{dl} (° cm$^{1/2}$)

164   can be given as

165
$$\sigma_{dl} = \sqrt{dl} * \sigma. \tag{4}$$

166   In this way, the deflection from the original root tip location does not depend on the spatial resolution of the root

167   growth model. By using the maximum root segment length as normalization factor for the standard deviation of the

168   random deflection angle, we create a dependency between σ_{dl} and soil penetration resistance. In this way,

169   experimental observations of higher root tortuosity in more compact soil (Tracy 2013) are taken into account.

170

7

171   Mathematical formulation of the anisotropy approach to model changes in root growth direction

172   We implemented our new model approach in the three dimensional numerical R-SWMS model (Javaux et al. 2008).

173   This model couples the root growth model by Clausnitzer and Hopmans (1994) with a model that simulates water

174   flow in the soil domain and in the root system (Doussan et al. 1998; Richards 1931). For the numerical solution of

175   the water flow equation, the soil domain is discretized in a regular cubic grid of nodes. Initial soil hydraulic

176   properties and soil bulk density are user defined input values and given explicitly for each node of the grid. The

177   system of root branches consists of straight root segments. At each root growth time step, a new root segment

178   emerges from the tip of a growing branch and moves the root apex to a new position. Length and orientation of the

179   newly developed root segment are influenced by a soil mechanical conductance tensor and a root inherent driving

180   force (equation (1)).

181   Soil penetration resistance in the bulk soil is calculated for each grid node as a function of soil bulk density, soil

182   water potential and effective saturation using the pedotransfer function developed by Whalley et al. (2007):

183     $$\log_{10} R = 0.35 * \log_{10}(|\psi| * S_e) + 0.93 * \rho_b + 1.26, \tag{5}$$

184   where R is the soil penetration resistance (kPa), ψ the water potential (kPa), S_e the effective saturation (-) and ρ_b the

185   soil bulk density (g cm^{-3}). This pedotransfer function is based on the analysis of 12 different soils with varying bulk

186   density and organic carbon, sand, silt and clay contents and can thus be assumed to be valid for a wide range of soils.

187   Soil mechanical conductance k (kPa^{-1}) is then determined as the inverse of soil penetration resistance R:

188     $$k = \frac{1}{R} \; . \tag{6}$$

189   Soil penetration resistances respectively soil mechanical conductances are specified at each node of a grid cell. We

190   assume that these nodal soil mechanical conductances are direction independent or isotropic properties. The eight

191   nodal conductances of the grid cell in which the root tip is located are used to determine an average or grid cell

192   conductance tensor (equation (2)), which is assumed to be constant within the grid cell. Homogeneous nodal root

193   conductances lead to an isotropic soil mechanical conductance.

194   In a regular cubic soil grid, macropores are designed in a stepwise structure by arranging grid cells on top or next to

195   each other (Fig. 2). For whichever inclination angle of the macropore, the principal axes of anisotropy then either

196 coincide with or stand at an angle of 45 ° to one of the three axes of the Cartesian coordinate system. If macropores

197 are the cause of soil anisotropy, it is thus sufficient to only consider four possible orientations of the axes of

198 anisotropy. Rotating the Cartesian coordinate system by 45° around each one of its main axes gives us three local

199 coordinate systems of anisotropy (Fig. 3). For each root tip, we then calculate four different conductance tensors and

200 choose the one for which the contrast between the main axes of anisotropy is largest.

201 In the simplest case where the main axes of anisotropy coincide with the axes of the Cartesian coordinate system, the

202 conductance tensor is calculated as follows: In all three directions of the Cartesian coordinate system, the grid cell is

203 virtually cut into two halves, which are regarded as two separate soil layers with different conductances. The average

204 soil conductance of each half space of one grid cell is calculated as the arithmetic mean of the conductance values of

205 the four corner nodes located within this half (Fig. 4, equation (7)):

$$\text{kh}_{x1} = \frac{k_1 + k_2 + k_3 + k_4}{4} \, . \tag{7}$$

207 Each axis of the Cartesian coordinate system is aligned perpendicular to two half spaces of a grid cell. In line with

208 hydraulic conductivity, the average conductance for each direction is calculated as the harmonic mean of the

209 conductances of two opposing half spaces of a grid cell (Fig. 5, equation (8)).

$$\text{k}_{xx} = \frac{2}{\frac{1}{\text{kh}_{x1}} + \frac{1}{\text{kh}_{x2}}} \, . \tag{8}$$

211 In case that the main axes of anisotropy do not coincide with axes of the Cartesian coordinate system, we calculate

212 the average soil conductance for each grid cell half perpendicular to the axes of the rotated coordinate system. The

213 average soil conductance of the half space on either side of a rotated plane is the arithmetic mean of six weighted

214 conductances: While the conductances of the two corner nodes, which lie within one half are given the weight 1, the

215 conductances of the four corner nodes lying on the separating plane between two halves have the weight 0.5. The

216 average conductance for each direction is then once again calculated as the harmonic mean of the conductances of

217 two opposing grid cell halves. Fig. 6 and equations (9), (10) and (11) give an example for the calculation of the

218 conductance in y' – direction of the coordinate system that was rotated around the x-axis.

$$k'_{y1} = \frac{k_1 + k_2 + \frac{k_3}{2} + \frac{k_4}{2} + \frac{k_5}{2} + \frac{k_6}{2}}{4} \, , \tag{9}$$

9

220
$$k'_{y2} = \frac{k_7 + k_8 + \frac{k_3}{2} + \frac{k_4}{2} + \frac{k_5}{2} + \frac{k_6}{2}}{4},$$
(10)

221
$$k'_{yy} = \frac{2}{\frac{1}{k_{y'1}} + \frac{1}{k_{y'2}}},$$
(11)

222 where k'_{y1} and k'_{y2} are the average conductances of the rotated halves of a grid cell in y' direction, k_1 to k_8 are the

223 conductance values of the corner nodes of the grid cell and k'_{yy} is the conductance vector of the local coordinate

224 system, which was rotated around the x-axis in y' direction

225 The three conductance tensors in their local coordinate systems are then mapped back onto the Cartesian coordinate

226 system by the help of a rotation matrix (equation (12) following the approach by Lust (2001):

227
$$k = M_{rot} * k' * M'_{rot},$$
(12)

228 where **k** is the conductance tensor in the Cartesian coordinate system, **k'** is the conductance tensor in the local

229 coordinate system, $\mathbf{M_{rot}}$ is the rotation matrix and $\mathbf{M'_{rot}}$ is the conjugated rotation matrix.

230 The length of a newly developed root segment is calculated as the product of root elongation rate and a user defined

231 root growth time step. The root elongation rate E_r (cm d^{-1}) is assumed to be a function of soil strength. Bengough et

232 al. (2011) observed that the soil penetration resistance sufficient to stop root elongation completely (R_{max}, kPa) is a

233 function of matric potential (ψ, kPa) and can be calculated as

234
$$R_{max} = 4000 + 2.33 * |\psi|,$$
(13)

235 In the bulk soil, R_{max} corresponds approximately to the soil penetration resistance at the permanent wilting point ($\psi =$

236 -1500 kPa).The root elongation rate is assumed to decrease linearly between zero and maximum soil penetration

237 resistance. The actual root elongation rate can thus be calculated based on the fraction of the maximum root

238 elongation rate by

239
$$E_r = E_{max} * \left(1 - \frac{R_{eff}}{R_{max}}\right),$$
(14)

10

240   where E_r (cm d^{-1}) is the actual root elongation rate, E_{max} (cm d^{-1}) is the maximum root elongation rate and R_{eff} is the

241   effective soil penetration resistance in the direction of the root tip growth. R_{eff} is by definition the inverse of an

242   effective conductance in the direction of root growth k_{eff}:

243
$$R_{eff} = \frac{1}{k_{eff}};$$
(15)

244   k_{eff} is a function of both the average conductance of the grid cell and the root inherent growth direction and is

245   calculated as:

246
$$k_{eff} = |\mathbf{k} \cdot \widehat{\boldsymbol{F}}|,$$
(16)

247   where $\widehat{\boldsymbol{F}}$ is the unit length vector of the driving force. In this way, E_r is reduced stronger if the root grows

248   perpendicular to a hard soil layer than if it grows along a hard soil layer. This approach corresponds to observations

249   by Kolb et al. (2012) who found that radial constrictions applied to roots did not significantly reduce root elongation

250   rates, while axial constrictions did have a significant impact.

251

252   Model assumptions for root growth in macropores

253   In the case of a root growing within a grid cell at the interface between bulk soil and macropore, soil domain and

254   macropore are regarded as two soil regions with different soil mechanical conductances that influence the direction

255   in which the root will grow. The intensity with which a root is forced to grow towards the direction of higher

256   conductance depends on both the conductances in the bulk soil and in the macropore. While the conductance in the

257   bulk soil is calculated as the inverse of soil penetration resistance, the conductance in the macropore (k_{macro}) is

258   unknown. To identify plausible values of k_{macro}, we analyzed the anisotropy of one single grid cell with four bulk soil

259   and four macropore nodes. We define the degree of anisotropy (DA) according to Dal Ferro et al. (2014) as

260
$$DA = 1 - \frac{k_{perp}}{k_{long}},$$
(17)

261   where k_{perp} and k_{long} are the conductances perpendicular and along the macropore – bulk soil grid cell half spaces

262   (Fig. 7). A Da of 0 signifies perfect isotropy, while a DA of 1 represents maximum anisotropy. Fig. 8 shows the

263   influence of different parametrizations of k_{macro} on anisotropy for typical minimum and maximum values of soil

11

264 penetration resistance. Assuming that the conductance in the macropore is much higher than in the bulk soil,

265 anisotropy shall be well above 0. If the degree of anisotropy approaches 1, however, the influence of different soil

266 conductances is no longer perceptible. We therefore assume macropore conductance values of $1e4 \leq k_{macro} \leq 2e5$

267 kPa^{-1} as most plausible. The conductance in the macropore can be regarded as a sensitivity factor, which influences

268 the probability of a root to continue growing within the macropore or to re-enter the bulk soil.

269

270 Model setup

271 Using experimental model setups from literature, we built three simulation scenarios to assess the performance of our

272 new model approach.

273 Scenario 1: Visual comparison of simulation results with observed root growth patterns in structure soil

274 For our first simulation scenario, we used an experimental study by Stirzaker et al. (1996) on root growth of barley

275 (*Hordeum vulgare cv.* Yagan) in soil containing macropores at the plant root scale. The setup of the simulation

276 model was designed according to the descriptions by Stirzaker et al. (1996). Undescribed model parameters were

277 either taken from literature or approximated. The soil domain was a rectangular cuboid with a surface area of

278 8.7 x 8.7 cm² and a depth of 20.1 cm, which we discretized to cubic grid elements of 0.1 cm side length. The bulk

279 density of the boundary grid cells of the sides and the base of the soil domain were set to a virtual density of 4 g cm^{-3}

280 in order to simulate the impenetrable pot walls. Eight vertical macropores with a diameter each of 0.4 cm were

281 arranged symmetrically around the center of the soil domain on a circle with a radius of 2.5 cm (Fig. 9). We used the

282 soil properties of a sandy loam (table 1), which was packed to a bulk density of 1.77 g cm^{-3}. We did not consider soil

283 water flow and assumed hydrostatic equilibrium in the soil domain. The simulation runtime was set to 25 days.

284 The simulated root system consisted of seven axes from which one emerged at day zero, three at day one and three at

285 day three. The initial potential root elongation rate for barley was derived from literature (Materechera et al. 1991)

286 and set to 1.2 cm d^{-1}. Watt et al. (2006) observed the growth rates of roots to decrease with time and branch roots to

287 grow more slowly than their parent axes. We thus reduced the elongation rate for 8 day old first order roots to 0.8 cm

288 d^{-1}. Root images by Stirzaker et al. (1996) show that roots grew in a low angle from the horizontal over the whole

289 width of the pot before they turn downwards (Fig. 11 (a)). In order to reproduce these root growth patterns,

290 sensitivity to gravitropism was set to the extremely low value of 0.005 for 1st order roots. Rose (1983) observed roots

12

291   of higher branching to be less gravitropic. Sensitivity to gravitropism for 2nd and 3rd order roots was thus reduced to

292   0.001. The root tortuosity as displayed in Fig. 11 (a) could be best reproduced with unit standard deviations of the

293   random angle of 45 °. The initial growth angle for axial roots was set to 0 °; the branching angle (relative to the

294   parent roots) to 90 °. Branch spacing was estimated and set to a value of 0.6 days for 1st order roots and 0.4 days for

295   2nd order roots.

296   Root water uptake was not considered in the simulations. Soil water potentials were set so that simulated soil

297   penetration resistances matched experimentally measured ones. We chose a whole pot matrix potential of -100 kPa,

298   which resulted in soil penetration resistances of 2500 kPa and corresponded approximately to the experimentally

299   observed values by Stirzaker et al. (1996), which lay between 2000 and 4000 kPa. The complete parameter set is

300   presented in table 2, while the values for the different parametrizations are presented in table 3.

301   Scenario 2: Quantitative comparison of simulation and experimental results on single root growth in inclined

302   macropores

303   For our second simulation scenario, we used an experimental study by Hirth et al. (2005) on the ability of seedling

304   roots of rye grass (*Lolium perenne L.)* to penetrate the soil from artificial macropores under varying soil bulk

305   densities and macropore inclination angles. The setup of the simulation model was designed according to the

306   descriptions by Hirth et al. (2005). Undescribed model parameters were either taken from literature or approximated.

307   The rectangular-shaped soil domain had a surface area of 3 x 1 cm² and a depth of 3 cm, which we discretized to

308   cubic grid cells of 0.1 cm side length. One single macropore with an angle of 40 ° respectively 90 ° was inserted into

309   the soil domain. Macropore and interface had a horizontal cross section area of 0.09 cm². The seed (starting point of

310   the root tip) was placed at the edge of the macropore (Fig. 10). We used the soil properties of a silty loam with the

311   texture indicated in table 1. The soil was packed to uniform bulk densities of 1.25, 1.38 and 1.50 g cm⁻³. In

312   accordance with the experimental setup, macropore wall compaction was not considered. Hirth et al. (2005) kept the

313   matric potential in the soil cores at a constant value of -5 kPa by connecting them to 0.5 m hanging columns of

314   water. We therefore assumed that root water uptake does not significantly affect the surrounding soil and performed

315   simulations without root water uptake. We did not consider soil water flow and assumed hydrostatic equilibrium in

316   the soil domain. The simulation runtime was set to 7 days.

317 The simulation of only one single root without laterals reduced the required input parameters for root growth to

318 potential root elongation rate, sensitivity to gravitropism, unit standard deviation of the random deflection angle and

319 conductance in the macropore. A potential root elongation rate of 0.49 cm d^{-1}, which we assumed to stay constant

320 over time was best suited to reproduce the actual root lengths measured by Hirth et al. (2005). This value is within

321 the range of the standard error of the mean of the potential root elongation rate for seedlings of annual ryegrass

322 (*L.rigidum*) given by Materechera et al. (1991). The remaining root growth parameters were not experimentally

323 determined and thus unknown. To evaluate the influence of different root growth parametrizations, we performed

324 simulations with different combinations of these parameters (see table 3 for chosen parameter values). Altogether,

325 we carried out 576 different simulations, which were the factorial combinations of three bulk densities, two

326 macropore angles and a control soil domain without macropore, four sensitivities to gravitropism (sg), four unit

327 standard deviations of the random deflection angle (σ) and four conductances in the macropore (k$_{macro}$). The

328 complete parameter set is presented in table 2.

329 To obtain representative simulation results of the stochastic process, which is generated by the random deflection

330 angle, we performed 100 replicates of each simulation using different random seed numbers. Experimental results

331 reported by Hirth et al. (2005) represent the average of 24 replicates, but no information of standard deviations was

332 provided.

333 Scenario 3: Virtual simulation experiment on root growth in a compacted subsoil layer that contains macropores

334 For our third simulation scenario, we carried out a simulation experiment on single root growth in a two - layered

335 soil domain where the compacted subsoil contained macropores. The simulation experiment represents the case of

336 root growth in soil with a plough. The soil domain was a rectangular cuboid of 3 cm side length in each direction,

337 which we discretized to cubic grid cells of 0.1 cm side length. We implemented two different soil layers into this soil

338 cube: a topsoil layer with a bulk density of 1.25 g cm^{-3} in the upper 1.5 cm of the cube and an impenetrable subsoil

339 layer with a bulk density of 3 g cm^{-3} in the lower 1.5 cm of the cube. Additionally, we inserted eight macropores into

340 the compacted subsoil layer. They were aligned symmetrically in a square with a distance of 0.9 cm to the borders of

341 the soil cube (Fig. 15). Each macropore was made up of nine grid nodes with macropore properties. We used root

342 growth parameters from the previous example for rye grass (*Lolium perenne L.*) with a sensitivity to gravitropism of

343 0.05 and a unit standard deviation of the random angle of 45 °. Root water uptake was not included. We did not

14

344 consider soil water flow and assumed hydrostatic equilibrium in the soil domain. The simulation runtime was set to

345 10 days. We performed only one simulation. The complete parameter set is presented in table 2.

346 **Results**

347 Scenario 1: Visual comparison of simulation results with observed root growth patterns in structure soil

348 We used both the tropism and anisotropy approach in order to simulate the experimental observations by Stirzaker et

349 al. (1996). The quality of the simulation results was evaluated visually by comparing 2D-images of the simulated and

350 the experimental root systems and quantitatively by comparing total root lengths and root length density profiles

351 (RLD profiles).

352 Both approaches led to simulation results where the roots predominantly did use macropores as preferential growth

353 pathways. The root growth behavior within macropores, however, was different: Using the tropism approach, the

354 roots only slowly grew downwards while spiraling horizontally over the whole cross section of the macropore; using

355 the anisotropy approach, the roots grew straight downwards along the pore wall, which better captures experimental

356 observations (Fig. 11). The simulation results in Fig. 11 are displayed in a layout so as to resemble the original figure

357 from Stirzaker et al. (1996), Fig. 6c. We found a total root length of 750 cm for the simulated root system, which

358 corresponds well to the experimentally observed one of 720 cm.

359 We determined the RLD profile from the original 2D image from Stirzaker et al. (1996), Fig. 6c with the help of the

360 image analysis tool Root System Analyzer (Leitner et al. 2014) and compared it with the RLD profiles of the

361 simulated 3D root systems (Fig. 12). It must be noted that the RLD profile obtained from the 2D image from

362 Stirzaker et al. (1996) can only be an approximation of the RLD profile of the real root system due to low image

363 resolution and the two dimensional representation of a three dimensional root system. The RLD profile produced

364 with the anisotropy approach was able to capture the larger root length density in the upper 5 cm of the soil domain,

365 which then decreased sharply. The RLD profile produced with the tropism approach largely overestimated RLD in

366 the upper soil domain, while underestimating it in the lower soil domain. The root length density within macropores

367 (area between the dashed and the solid line) as a percentage of total RLD was similar for the experimental RLD

368 profile (26 %) and the simulated RLD profile produced with the anisotropy approach (21 %).

15

369   Scenario 2: Quantitative comparison of simulation and experimental results on single root growth in inclined

370   macropores

371   Simulation and experimental results by Hirth et al. (2005) were compared quantitatively. We used the characteristics

372   total root length (cm) and root length fraction that remained within the macropore (%) as a means of comparison

373   between experiment and simulation. The variability of the averaged results of different simulations is caused by

374   different parameter combinations, while the variability of the individual results is the random variation between the

375   100 replicate simulations.

376   *Influence of different macropore inclination angles and different bulk densities*

377   Fig. 13 shows a comparison between the simulation results obtained with a randomly chosen parametrization (sg =

378   0.05, σ = 45 °, k_{macro} = 8e4 kPa^{-1}), and the experimental results by Hirth et al. (2005) for a smooth macropore wall.

379   The simulations captured well the experimental observations of increasing root length fractions within the macropore

380   with an increasing macropore inclination angle from the horizontal. In accordance with the experimental

381   observations, different levels of bulk density only had an effect on the roots growing in the 40 ° inclined macropores.

382   Simulations were able to reproduce the experimentally observed increase in root length fractions within the

383   macropore for increasing levels of bulk density. Due to this increase, total root lengths did not decrease for

384   increasing levels of bulk density. Compared to root growth in a homogeneous soil domain with equal bulk density,

385   the presence of macropores increased total root lengths by 20 % to 40 %.

386   *Quantitative simulation results: 90 ° - inclined macropore*

387   In the case of a 90 ° inclined (vertical) macropore, all simulated roots remained within the macropore for all different

388   parameter combinations. They reached average root lengths between 2.8 cm and 3.3 cm and thus grew at 83 % to

389   98 % of the potential root elongation rate. These results correspond well to the findings by Hirth et al. (2005) who

390   measured average root length fractions in macropores between 83 % and 90 % and total root lengths between 2.9 cm

391   and 3.1 cm.

392   *Quantitative simulation results: 40 ° - inclined macropore*

16

393   In the case of a macropore with 40 ° inclination, the simulated average root length fraction within a macropore

394   reached – depending on the parametrization - values between 18 % and 60 %. Simulated averaged total root lengths

395   ranged from 2.5 cm to 3.0 cm. The root thus grew at 74 % to 89 % of the potential root elongation rate. Hirth et al.

396   (2005) found – depending on the roughness of the macropore walls – root length fractions within macropores

397   between 14 % and 86 % and total root lengths between 1.9 cm and 3.0 cm. Both simulated root length fractions

398   within macropores and total root lengths were thus in acceptable agreement with experimental results.

399   *Influence of different parametrizations on the simulation results of the 40 ° inclined macropore*

400   Fig. 14 gives an overview of the influence of different parametrizations (table 3) on simulated root length fractions

401   remaining within a 40 ° inclined macropore. Different parametrizations of bulk density and conductance in the

402   macropore (k_{macro}) were pooled in the parameter 'degree of anisotropy' (Fig. 7, equation (17)).

403   To evaluate the influence of different degrees of anisotropy on root length fractions remaining within the macropore,

404   we fitted linear regression lines to the simulation results of each parameter combination. As expected, increasing

405   degrees of anisotropy led to an increase in root length fractions within a macropore for nearly all parameter

406   combinations. The coefficients of determination show that the variability of the simulation results increased both

407   with increasing standard deviations of the random angle and decreasing sensitivities to gravitropism. For parameter

408   combinations including a sensitivity of gravitropism of 0.005, no regression line could be fitted due to the high

409   variability of the simulation results. There is a trend of increasing root length fractions and decreasing rates of

410   increase both with increasing standard deviations of the random angle and decreasing sensitivities to gravitropism,

411   but the pattern is not consistent. For individual simulations, root length fractions within macropores of up to 100 %

412   could be reached; the maximum value for the intercept of a regression line with a degree of anisotropy of 1, however,

413   was only 50 %.

414   *Influence of the roughness of macropore walls*

415   Hirth et al. (2005) performed experiments with smooth and scarified macropore wall reliefs. They found significant

416   differences in both root length fractions within macropores and total root lengths for the two different treatments.

417   Larger root length fractions remained within the smooth macropore (averaged over all bulk density levels, 68 %)

418   than within the scarified macropore (averaged over all bulk density levels, 38 %). Consequently, total root lengths

17

419   were larger for roots growing in smooth macropores (on average 2.85 cm) than for roots growing in scarified

420   macropores (on average 2.3 cm). In the simulation model, it is not possible to directly take into account macropore

421   wall roughness. However, the influence of wall roughness can be controlled indirectly via the conductance in the

422   macropore. In the parametrization example from Fig. 13, an increase of k_{macro} from 2e4 kPa^{-1} to 8e4 kPa^{-1} led to an

423   increase in the average root length fraction within the macropore from 33 % to 44 % if averaged over all bulk density

424   levels.

425   Scenario 3: Virtual simulation experiment on root growth in a compacted subsoil layer that contains macropores

426   The simulation result produced with the anisotropy approach captured well the expected root growth behavior (Fig.

427   15 (b)). When reaching the compacted subsoil layer, the root grew horizontally along it keeping constant contact to

428   the soil layer until it encountered a macropore. It then entered the pore and grew straight down along the pore wall.

429   Using the tropism approach (Fig. 15 (a)), the root was not able to enter the macropore, but oscillated around its

430   opening without entering it.

431   **Discussion**

432   Concepts of root growth models and their parameters are difficult or even impossible to validate or derive from

433   direct measurements. However, by comparing simulated root architectures with experimentally observed ones,

434   different concepts can be compared with each other and more appropriate ones can be identified. In this study we

435   demonstrated that our new anisotropy approach to simulate changes in root growth direction due to soil penetration

436   resistance is more appropriate to describe the development of root systems in soil with macropores. Data from

437   experiments in which parameters like the macropore inclination angle and the matric bulk density were

438   systematically varied could be used to constrain parameters of the root growth model. It must be noted that these

439   experiments were not designed with the purpose of calibrating or validating a root growth model. Using a simulation

440   model to design or plan such experiments could be beneficial to measure variables that contain additional

441   information and allow a better determination of model parameters. In this example, the variability of root lengths and

442   root length fractions within macropores could have been an additional source of information since it differed strongly

443   between simulations using different parameter values.

18

444   Hirth et al. (2005) showed that the roughness of macropore walls has a significant influence on the probability of a

445   root to continue growing within a macropore or to re - enter the bulk soil. For the simulation of roots growing in

446   natural macropore networks, knowledge about the macropore wall roughness is thus mandatory. Combined

447   information on root growth in macropores and on the roughness of earthworm burrow walls or root channels such as

448   provided by Leue and Gerke (2016) could be used to calibrate the simulation model in that way.

449   Macropore walls were observed to be richer in nutrients than the surrounding bulk soil (Athmann et al. 2014; Barej

450   et al. 2014; Jiménez et al. 2003). For simulations of root growth in macropores including nutrient uptake, information

451   about the root – macropore wall contact is thus essential.

452   The new model approach was developed for a simulation domain that is discretized into a regular cubic grid of

453   nodes. If used in a model with a different description of the simulation domain, an alternative approach must be

454   devised for the calculation of soil mechanical conductances. An example for such a model is RootBox (Leitner et al.

455   2010), where soil physical properties are not assigned to grid nodes, but implemented in a lattice-free way using

456   signed distance functions.

457   For simulations of root growth in macropores on a scale larger than the single root scale, we rely on extensive

458   experimental data to parametrize and validate the model. Non – invasive methods such as rhizotron studies

459   (Kuchenbuch and Ingram 2002; Nagel et al. 2012; Tracy et al. 2010) may provide reliable information on root

460   elongation rates and root growth parameters. Imaging methods such as X-ray computed tomography (Rab et al.

461   2014; Tracy et al. 2010) or magnetic resonance imaging (Gruwel 2014; Stingaciu et al. 2013) can be used to

462   characterize the spatial distribution of both macropore networks and plant roots in 3D and additionally to visualize

463   and quantify soil water dynamics including preferential flow (Sammartino et al. 2015).

464   Our new anisotropy approach to model the effect of macropores on root growth direction is part of the mechanistic

465   3D model for water and solute transport in the soil-root system, R-SWMS (Javaux et al. 2008). Thus, it is a

466   contribution to a better understanding of underlying processes and feedback loops of soil - plant interactions on the

467   root system scale.

19

472   **References**

473   Athmann M, Huang N, Kautz T, Köpke U 2014 Biopore characterization with in situ endoscopy: Influence of

474   earthworms on carbon and nitrogen contents. In: RGA U (ed) 4th ISOFAR Scientific Conference, Istanbul.

475   Athmann M, Kautz T, Pude R, Köpke U 2013 Root growth in biopores—evaluation with in situ endoscopy. Plant and

476   Soil 371: 179-190. doi: 10.1007/s11104-013-1673-5.

477   Bao Y, Aggarwal P, Robbins NE, Sturrock CJ, Thompson MC, Tan HQ, Tham C, Duan L, Rodriguez PL, Vernoux T 2014

478   Plant roots use a patterning mechanism to position lateral root branches toward available water.

479   Proceedings of the National Academy of Sciences 111: 9319-9324.

480   Barej JAM, Pätzold S, Perkons U, Amelung W 2014 Phosphorus fractions in bulk subsoil and its biopore system.

481   European Journal of Soil Science 65: 553-561.

482   Bear J 2013 Dynamics of fluids in porous media. Courier Corporation.

483   Bengough A, McKenzie B, Hallett P, Valentine T 2011 Root elongation, water stress, and mechanical impedance: a

484   review of limiting stresses and beneficial root tip traits. Journal of Experimental Botany 62: 59-68. doi:

485   10.1093/jxb/erq350.

486   Clausnitzer V, Hopmans J 1994 Simultaneous modeling of transient three-dimensional root growth and soil water

487   flow. Plant and soil 164: 299-314.

488   Dal Ferro N, Sartori L, Simonetti G, Berti A, Morari F 2014 Soil macro-and microstructure as affected by different

489   tillage systems and their effects on maize root growth. Soil and Tillage Research 140: 55-65.

490   Dexter A 1986 Model experiments on the behaviour of roots at the interface between a tilled seed-bed and a

491   compacted subsoil. Plant and Soil: 149-161.

492   Dexter A, Hewitt J 1978 The deflection of plant roots. Journal of agricultural Engineering Resources 23: 17-22.

20

493 Doussan C, Vercambre G, Pagès L 1998 Modelling of the Hydraulic Architecture of Root Systems: An integrated

494   Approach to Water Absorption - Distribution of Axial and Radial Conductances in Maize. Annals of Botany

495   81: 225-232.

496 Ehlers W, Köpke U, Hesse E, Böhm W 1983a Penetration resistance and root growth of oats in tilles and untilled

497   Loess soil. Soil & Tillage Research 3: 261-275.

498 Ehlers W, Köpke U, Hesse F, Böhm W 1983b Penetration resistance and root growth of oats in tilled and untilled

499   loess soil. Soil and Tillage Research 3: 261-275.

500 Gaiser T, Perkons U, Küpper PM, Kautz T, Uteau-Puschmann D, Ewert F, Enders A, Krauss G 2013 Modeling biopore

501   effects on root growth and biomass production on soils with pronounced sub-soil clay accumulation.

502   Ecological Modelling 256: 6-15.

503 Gregory PJ 2008 Plant roots: growth, activity and interactions with the soil. John Wiley & Sons.

504 Gruwel ML 2014 In situ magnetic resonance imaging of plant roots. Vadose Zone Journal 13.

505 Hatano R, Iwanaga K, Okajima H, Sakuma T 1988 Relationship between the distribution of soil macropores and root

506   elongation. Soil Science and Plant Nutrition 34: 535-546.

507 Hirth J, McKenzie B, Tisdall J 2005 Ability of seedling roots of Lolium perenne L. to penetrate soil from artificial

508   biopores is modified by soil bulk density, biopore angle and biopore relief. Plant and Soil 272: 327-336. doi:

509   10.1007/s11104-004-5764-1.

510 Jakobsen B, Dexter A 1988 Influence of biopores on root-growth, water-uptake and grain-yield of wheat (triticum-

511   aestivum) based on predictions from a computer-model. Biol Fertil Soils 6: 315-321.

512 Javaux M, Schröder T, Vanderborght J, Vereecken H 2008 Use of a Three-Dimensional Detailed Modeling Approach

513   for Predicting Root Water Uptake. Vadose Zone Journal 7: 1079-1079.

514 Jiménez JJ, Cepeda A, Decaëns T, Oberson A, Friesen DK 2003 Phosphorus fractions and dynamics in surface

515   earthworm casts under native and improved grasslands in a Colombian savanna Oxisol. Soil Biology and

516   Biochemistry 35: 715-727.

517 Kautz T, Amelung W, Ewert F, Gaiser T, Horn R, Jahn R, Javaux M, Kemna A, Kuzyakov Y, Munch J, Patzold S, Peth S,

518   Scherer H, Schloter M, Schneider H, Vanderborght J, Vetterlein D, Walter A, Wiesenberg G, Kopke U 2013a

21

519   Nutrient acquisition from arable subsoils in temperate climates: A review. Soil Biol Biochem 57: 1003-

520   1022. doi: 10.1016/j.soilbio.2012.09.014.

521 Kautz T, Köpke U 2009 Assessing the root-soil contact in biopores. International Symposium 'Root Research and

522   Applications', Vienna, Austria.

523 Kautz T, Perkons U, Athmann M, Pude R, Köpke U 2013b Barley roots are not constrained to large-sized biopores in

524   the subsoil of a deep Haplic Luvisol. Biol Fertil Soils 49: 959-963. doi: 10.1007/s00374-013-0783-9.

525 Kirkegaard J, Lilley J, Howe G, Graham J 2007 Impact of subsoil water use on wheta yield. Australian Journal of

526   Agricultural Research 58: 303-315.

527 Kolb E, Hartmann C, Genet P 2012 Radial force development during root growth measured by phytoplasticity. .

528   Plant and Soil 360: 19-35.

529 Kuchenbuch R, Ingram K 2002 Image analysis for non-destructive and non-invasive quantification of root growth

530   and soilw ater content in rhizotrons. Journal of Plant Nutrition and Soil Science 165: 573-581.

531 Kuhlmann H, Baumgärtel G 1991 Potential importance of the subsoil for the P and Mg nutrition of wheat. Plant and

532   Soil 137: 259-266.

533 Laloy E, Weynants M, Bielders C, Vanclooster M, Javaux M 2010 How efficient are one-dimensional models to

534   reproduce the hydrodynamic behavior of structured soils subjected to multi-step outflow experiments?

535   Journal of Hydrology 393: 37-52.

536 Leitner D, Klepsch S, Bodner G, Schnepf A 2010 A dynamic root system growth model based on L-Systems. Plant

537   and Soil 332: 177-192.

538 Leue M, Gerke HH 2016 Roughness of biopores and cracks in Bt-horizons assessed by confocal laser scanning

539   microscopy. Journal of Plant Nutrition and Soil Science.

540 Lust M 2001 Quaternionen- mathematischer Hintergrund und ihre Interpretation als Rotationen. In: U Koblenz-

541   Landau (ed).

542 Materechera S, Dexter A, Alston A 1991 Penetration of very strong soils by seedling roots of different plant species.

543   Plant and Soil 135: 31-34.

544   McKenzie B, Bengough A, Hallett P, Thomas W, Forster B, McNicol J 2009 Deep rooting and drought screening of

545   cereal crops: A novel field-based method and its application. Field Crop Res 112: 165-171. doi:

546   10.1016/j.fcr.2009.02.012.

547   Nagel K, Putz A, Gilmer F, Heinz K, Fischbach A, Pfeifer J, Faget M, Bloßfeld S, Ernst M, Dimaki C, Kastenholz B,

548   Kleinert A, Galinski A, Scharr H, Fiorani F, Schurr U 2012 GROWSCREEN-Rhizo is a novel phenotyping robot

549   enablign simultaneous measruements of root and shoot growth for pkants grown in soil-filled rhizotrons.

550   Functional Plant Biology 39: 891-904.

551   Pagès L, Vercambre G, Drouet J-L, Lecompte F, Collet C, Le Bot J 2004 Root Typ: a generic model to depict and

552   analyse the root system architecture. Plant and Soil 258: 103-119.

553   Rab M, Haling R, Aarons S, Hannah M, Young I, Gibson D 2014 Evaluation of X-ray computed tomography for

554   quantifying macroporosity of loamy pasture soils. Geoderma 213: 460-470.

555   Richards L 1931 Capillary conduction of liquids through porous medium. Physics 1: 318-333.

556   Rose D 1983 The description of teh growth of root systems. Plant and Soil 75: 405-415.

557   Sammartino S, Lissy A-S, Bogner C, Van Den Bogaert R, Capowiez Y, Ruy S, Cornu S 2015 Identifying the functional

558   macropore network related to preferential flow in structured soils. Vadose Zone Journal 14.

559   Shkolnik D, Krieger G, Nuriel R, Fromm H 2016 Hydrotropism: root bending does not require auxin redistribution.

560   Molecular plant 9: 757-759.

561   Stewart J, Moran C, Wood J 1999 Macropore sheath: quantification of plant root and soil macproe association.

562   Plant and Soil 211: 59-67.

563   Stingaciu L, Schulz H, Pohlmeier A, Behnke S, Zilken H, Javaux M, Vereecken H 2013 In situ root system architecture

564   extraction from magnetic resonance imaging for water uptake modeling. Vadose zone journal 12.

565   Stirzaker R, Passioura J, Wilms Y 1996 Soil structure and plant growth: Impact of bulk density and biopores. Plant

566   and soil 185: 151-162.

567   Toyota M, Gilroy S 2013 Gravitropism and mechanical signaling in plants. American journal of botany 100: 111.

568   Tracy S 2013 The response of root system architecture to soil compaction. Philosophy. Nottingham.

569   Tracy SR, Roberts JA, Black CR, McNeill A, Davidson R, Mooney SJ 2010 The X-factor: visualizing undisturbed root

570   architecture in soils using X-ray computed tomography. Journal of experimental botany 61: 311-313.

23

571   Tsutsumi D, Kosugi K, Mizuyama T 2003 Root-system development and water-extraction model considering

572   hydrotropism. Soil Science Society of America Journal 67: 387-401.

573   Valentine T, Hallet P, Binnie K, Young M, Squire G, Bengough G 2012 Soil strength and macropore volume limit root

574   elongation rates in many UK agricultural soils. Annals of Botany 110: 259-270.

575   Vereecken H, Schnepf A, Hopmans JW, Javaux M, Or D, Roose T, Vanderborght J, Young M, Amelung W, Aitkenhead

576   M, Allison SD, Assouline S, Baveye P, Berli M, Brüggemann N, Finke P, Flury M, Gaiser T, Govers G,

577   Ghezzehei T, Hallett PD, Hendricks Franssen HJ, Heppel J, Horn R, Huisman J, Jacques D, Jonard F, Kollet S,

578   Lafolie F, Lamorski K, Leitner D, Mc Bratney A, Minasny B, Montzka C, Nowak W, Pachepsky Y, Padarian J,

579   Romano N, Roth K, Rothfuss Y, Rowe E, Schwen A, Simunek J, Tiktak A, Van Dam J, van der Zee S, Vogel H,

580   Vrugt J, Wöhling T, Young I 2016 Modeling Soil Processes: Review, Key Challenges, and New Perspectives.

581   Vadose Zone Journal 15.

582   Watt M, Silk W, Passioura J 2006 Rates of root and organism growth, soil conditions, and temporal and spatial

583   developement of the Rhizosphere. Annals of Botany 97: 839-855.

584   Whalley W, To J, Kay B, Whitmore A 2007 Prediction of the penetrometer resistance of soils with models with few

585   parameters Geoderma 137: 370-377.

586   White R, Kirkegaard J 2010 The distribution and abundance of wheat roots in a dense, structured subsoil -

587   implications for water uptake. Plant Cell Environ 33: 133-148. doi: 10.1111/j.1365-3040.2009.02059.x.

588

24

Table 1: Texture of soils used in the simulation scenarios 1, 2 and 3

Simulation scenario	FAO soil classification	Sand (%)	Silt (%)	Clay (%)
Scenario 1	Sandy loam	74	12	14
Scenario 2 and 3	Silty loam	55.8	26.6	12.3

Table 2: Model parametrizations for simulation scenarios 1, 2 and 3

	Geometry of the soil domain					Root growth parameters								Simulation runtime
	L (cm)	W (cm)	D (cm)	ρ_b (g cm^{-3})	ψ (kPa)	E_{max} (cm d^{-1})	nbas (-)	basang (°)	brnang (°)	brspac (d^{-1})	σ (°)	sg (-)	k_{macro} (kPa^{-1})	(d)
Scenario1	8.7	8.7	20.1	1.77	-100	1.2 (0.8)	6	0	90	0.6 (0.4)	45	0.005 (0.001)	2.00E+05	25
Scenario2	3	1	3	Table 3	-5	0.68	-	-	-	-	Table 3	Table 3	Table 3	7
Scenario3	3	3	3	1.25 resp. 3	-15	0.68	-	-	-	-	45	0.05	1.00E+05	10

Values in parentheses indicate parametrizations for 2nd and 3rd order roots, L Length, W Width, ρ_b bulk density, ψ soil matric potential, E_{max} maximum elongation rate, *nbas* number of basal roots, *basing* basal root angle, *brnang* branching angle, *brspac* branch spacing, σ unit standard deviation of the random angle, *sg* sensitivity to gravitropism, k_{macro} conductance in the macropore

Table 3: Values for different parametrizations of scenario 2

| Inclination angle of the MP (°) | Soil bulk density, ρb (g cm^{-3}) | Root growth parameters | | |
		Sensitivity to gravitropism, sg (-)	Unit stdev of the random angle, σ (°)	Conductance in the MP, k_{macro} (kPa^{-1})
No macropore	1.25	0.005	5	2.00E+4
40	1.38	0.05	45	3.00E+4
90	1.50	0.1	90	5.00E+4
		0.2	180	8.00E+4

Fig. 1 Direction of the root segment expressed by the azimuth angle α with random deflection γ and the polar angle β with random deflection δ

Fig. 2 Stepwise structure of a 45 ° and a 60° inclined macropore

Fig. 3 Four local coordinate systems are sufficient to describe all possible main axes of anisotropy in a regular cubic grid. The planes perpendicular to the local coordinate axes are used to divide one cubic soil element in two half-spaces that are used to compute local average conductances (e.g. Fig. 5)

Fig. 4 Average conductance of one half space of a grid element perpendicular to the x- axis

Fig. 5 Conductance perpendicular to the conductances of the two half spaces

Fig. 6 Separating plane between two halves perpendicular to the y' – direction of the local coordinate system which was rotated around the x – axis

Fig. 7 The degree of anisotropy is one minus the ratio between the conductance perpendicular to (k_{perp}) and along (k_{long}) the plane that separates macropore from bulk soil and the bulk soil plane

Fig. 8 Influence of k_{macro} on the degree of anisotropy for typical minimum and maximum values of k_{soil}

Fig. 9 Side (a) and top (b) view of the soil domain with a 25 – day old barley root, scenario 1; the bulk soil is displayed in light grey, while the macropores are presented in dark grey and the root in black

Fig. 10 Soil domain, scenario 2; the bulk soil is displayed in light grey, while the macropores are presented in dark grey and the root in black

Fig. 11 Front view of barley roots growing in dense soil with macropores for 25 days: (a) Experimental results by Stirzaker et al. (1996), (b) Simulation results produced with the tropism approach, (c) Simulation results produced with the anisotropy approach

Fig. 12 Root length density profiles of barley roots growing in dense soil with macropores for 25 days: (a) RLD profile for original 2D image by Stirzaker et al. (1996), (b) RLD profile for simulated 3D root system produced with the tropism approach, (c) RLD profile for simulated 3D root system produced with the anisotropy approach

Fig. 13 Simulated and experimentally found relative root lengths within macropore and bulk soil; the first column (I) shows the simulation results obtained with a randomly chosen parametrization (sg= 0.05, σ=45 °, kmacro = 8e4 kPa-1), while the second (II) column illustrates the experimental results by Hirth et al. (2005). The different rows show results for different levels of soil bulk density (ρb low, ρb med, ρb high). The inclination angles of the colored lines represent the macropore inclination angles (40°, 90°); the different colors indicate the different locations of the root within the soil domain (macropore, bulk soil). The length of the colored lines represents the relative root length which is the total root length normalized with the length of a root growing in a soil domain with equal bulk density, but without macropore. Each line in the first column represents the average of 100 individual simulations. Each line in the second column represents the average of 24 individual simulations

Fig. 14 Influence of different parametrizations of sensitivity to gravitropism (sg), unit standard deviation of the random angle (σ) and degree of anisotropy on the fractions of root lengths remaining within a 40° inclined macropore. Each separate figure shows the results of 1200 individual simulations (100 replicates for 12 different degrees of anisotropy). R² specifies the coefficient of determination of the linear regression line that was fitted to the simulation results

Fig. 15 Soil domain and root simulated with the tropism (a) and the anisotropy (b) approach; the topsoil layer is presented in dark grey, the subsoil layer in light grey; the macropores are displayed in light grey and the root in black.
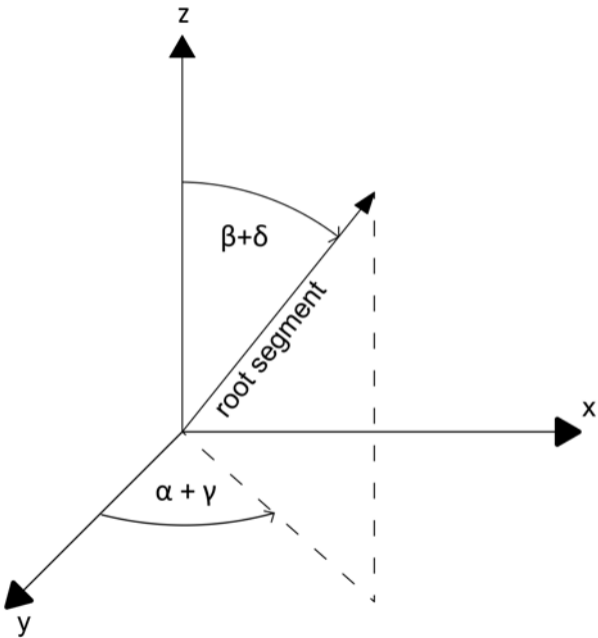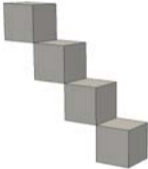
45° Rotation around

no rotation   x-axis   y-axis   z-axis

half space with average conductance kh_{x1}

half space with average conductance kh_{x1}
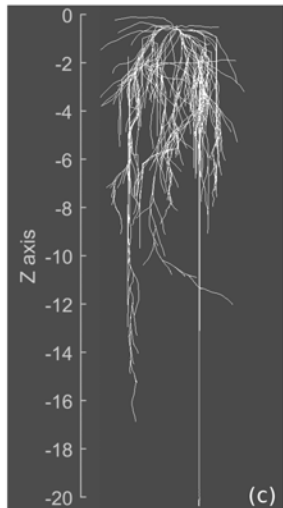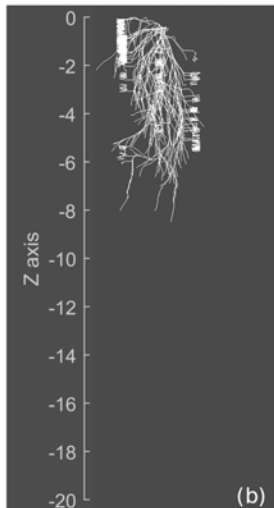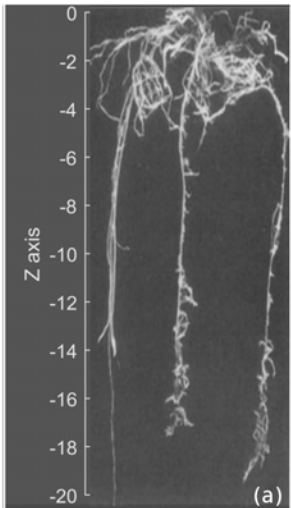
half space with average conductance kh_{x2}
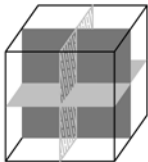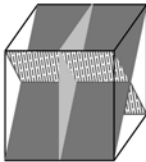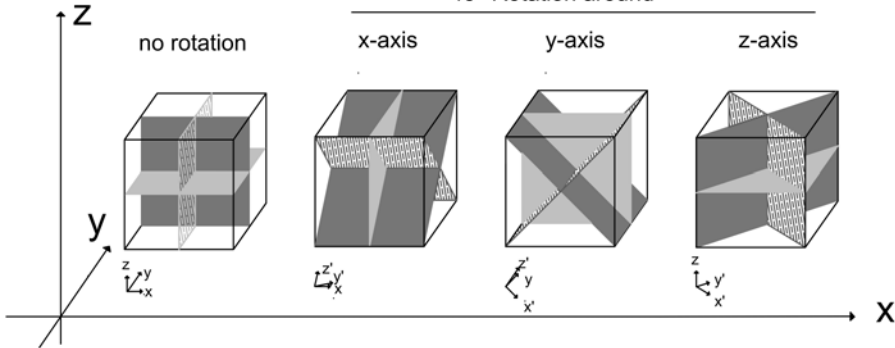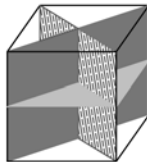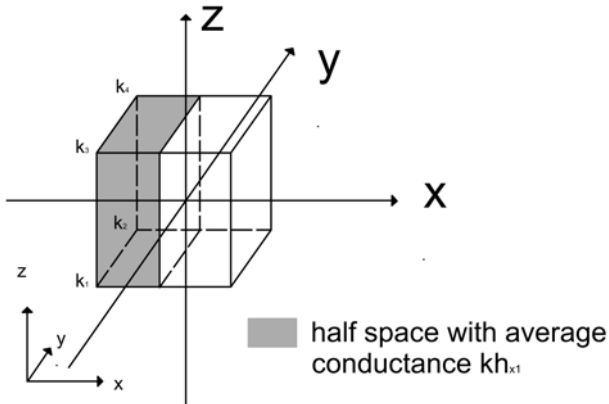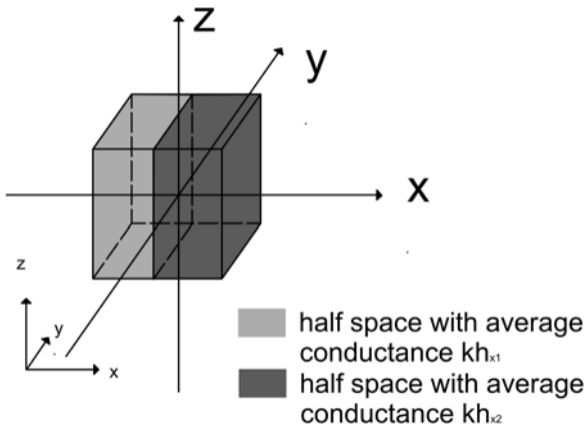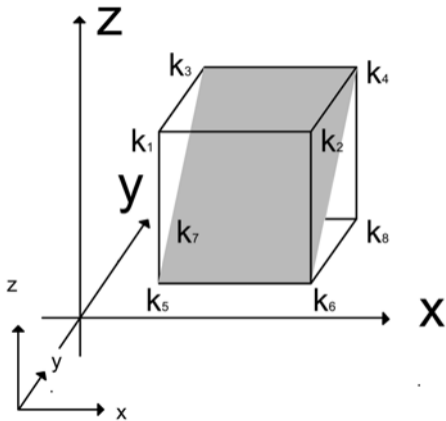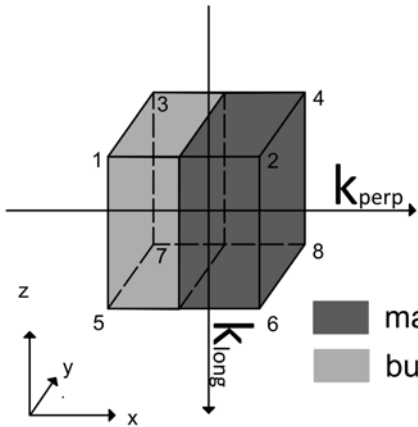
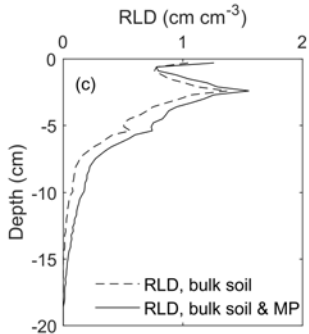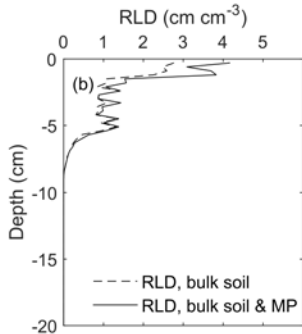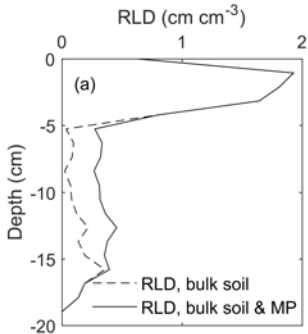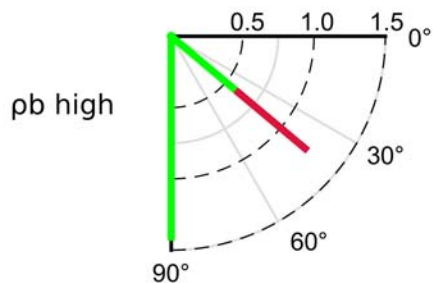macropore halfspace (nodes 2468)

bulk soil halfspace (nodes 1357)

(a)

(b)

Depth (cm)

Length (cm)

Width (cm)
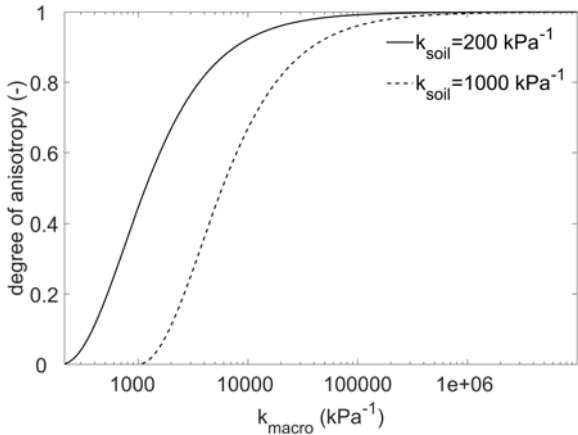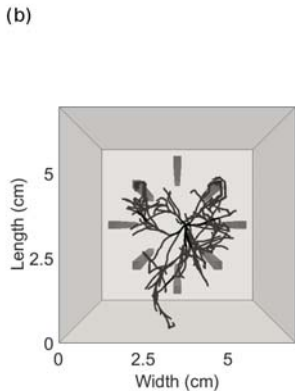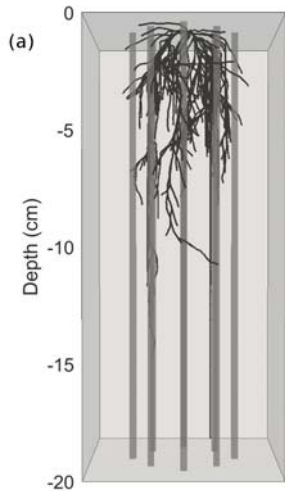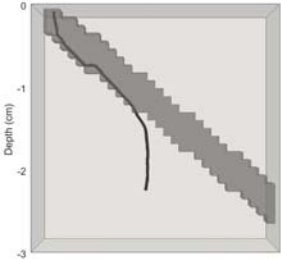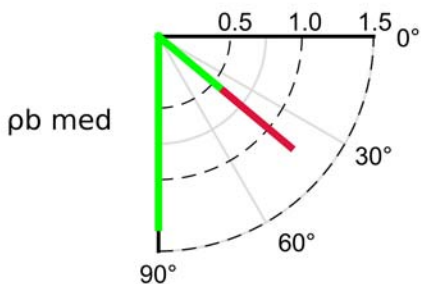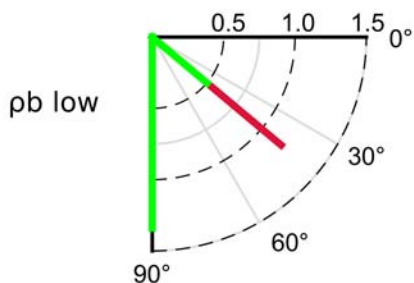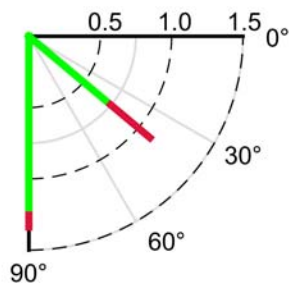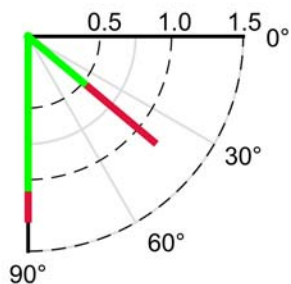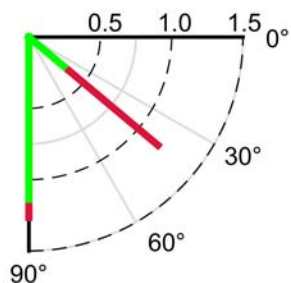
I. Simulation results   II. Experimental results

ρb low

ρb med

ρb high

Relative root length within the macropore
Relative root length within the bulk soil